Journal of Materials Science and Surface Engineering, 10: 1097-1103
ISSN (Online): 2348-8956; DOI: https://doi.org/10.52687/2348-8956/102

Peer Reviewed

Fabrication, Structural, Optical, Electrical and Gas Sensing Properties $CoAl_2O_4$ Doped Polypyrrole Nanocomposite Thin Films

Anita R. H · Nirdosh Patil

Department of Chemistry, Sharnbasva University, Vidya Nagar Kalaburagi, India.

ABSTRACT

The $CoAl_2O_4$ powder was produced in a double decomposition reaction involving solid $LiAlO_2$ and molten $KCoCl_3$ over a 24-hour period at 500°C. A series of conductive $CoAl_2O_4$ doped polypyrrole (PPy) nanocomposites thin films were synthesized by doping $CoAl_2O_4$ by weight percentage (10%, 20%, 30%, 40% and 50%) in aqueous solution of polypyrrole by chemical oxidative polymerization technique at room temperature. The produced Ppy-$CoAl_2O_4$ films were characterized by using deferent techniques such as the FTIR and XRD results confirmed the structural formation of Ppy-$CoAl_2O_4$ films from pyrrole monomer. Surface morphology (SEM) of Ppy-$CoAl_2O_4$ films have been found significant influence on the thermal stability and gas sensing properties. The electrical conductivity was measured by two probe technique. The investigation of thin films has shown higher conductivity of thin flims with increasing the dopant $CoAl_2O_4$ percentage. The optical characteristics of all evaluated films were examined, and it was found that when Ppy-$CoAl_2O_4$ content was increased, optical absorption decreased in both the VIS (500–700 nm) and UV (200–400 nm) wavelength ranges. The gas ammonia was utilised to examine how the examined films responded to gas detection.

ARTICLE HISTORY
Received 15-11-2022
Revised 04-01-2023
Accepted 01-04-2023
Published 22-12-2023

KEYWORDS
Polypyrrole
Ammonia gas
Morphology
Films
Spectroscopy

Introduction

The present world give a great emphasis on the study and development of nano size materials like a nanocomposite with excellent optical, electrical, chemical, and magnetic characteristics [1-4]. These properties are dissimilar from their constituent materials which make them a promising candidate for scientific and technical interests[5-9]. Researchers are developing a sort of techniques to reduce the particle size of the filler materials which simultaneously increase the surface area of the filler that is essential to transfer the load between the polymer matrix and the fillers. These nanocomposites may express a noticeable improvement on mechanical, thermal and electrical properties which are quite difficult to acquire from traditional micro scale fillers, for instance, aramid, glass or carbon fibers. Now a days electronics, automobile, aerospace, marine and other engineering industries show a great demand on these nanocomposites due to their outstanding mechanical and thermal properties. Ferrite is a specialised magnetic material class belonging from spinel group. They can be employed in microwave, transformer cores, magnetic memory, isolators, noise filters, etc. due to some of their excellent properties [10–13].

In particular, Hong et al. [14] created PPy/Pd nanocomposites in 2009 by first gas-phase polymerizing pyrrole and then reducing Pd ions in solution. The quantity of polymer additives, the length of the polymerization reaction, the concentration and ratio of reactants, and the composition of the composite membrane were all found to have a significant influence. They then calculated the nanocomposite's sensitivity to detect the presence NH_3. In this study, they showed that the size of Pd NPs and the arrangement of composite membranes had a substantial impact on the gas-sensing abilities of nanocomposites. The size of NPs can be decreased to less than 10 nm and improved distribution can be attained with the addition of PVP. Because the evenly distributed Pd NPs provided more active surface reaction sites and altered the charge transfer between the polymer and reaction gas molecules, the PPy and small-sized Pd-based gas sensors performed better than PPy alone. Zhang et al one-pot method was developed in 2013 to make PPy/Au nanocomposites with uniformly dispersed Au NPs on PPy. The addition of lysine significantly reduced the size of Au NPs. The hybrid system's NPs had an excellent consistency distribution in the meanwhile. The quantum size effect caused the Au NPs to become particularly active when they were smaller than 5 nm, which helped In the presence of atmospheric O_2, NH_3 molecules adsorb on the PPy sensor layer.At room temperature, PPy/Au nanocomposites had a sensitivity of roughly 1.47 for 300 ppm NH_3 detection. The homogeneous small-sized Au NPs dispersion was made possible by their contribution to the clearly improved sensor characteristics. Additionally, the potential mechanism was explored. PPy is a form of conducting polymer and a p-type semiconductor. The "nano Schottky effect" will be produced at the PPy/Au hybrid system's interface by the addition of Au NPs which will subsequently create a depletion layer, raising the resistance of the entire system The hybrid system's holes will be consumed and the resistance will increase in the presence of electron-doped NH_3.In present study we report the bi-metallic oxide ($CoAl_2O_4$) was used as dopant to the polypyrrole in order to obtain a new type of metal oxide doped polymer composite materials. Here, we present a procedure for the synthesis of $CoAl_2O_4$ nanoparticles, which further used as a filler material for the polypyrrole.

Corresponding Author: Anita R H, Tel: +22671409576
Email: anitahagaragi@gmail.com
Contents lists available at http://www.jmsse.in/ & http://www.jmsse.org/

The materials were examined using a variety of experimental approaches, and it was determined how $CoAl_2O_4$ nanoparticles affected the mechanical, thermal, optical, and electrical characteristics of composites made of $CoAl_2O_4$-doped polypyrrole (PPy-$CoAl_2O_4$).

Experimental

Chemical reagents

Starting materials included lithium carbonate Li_2CO_3 from Merck, γ-alumina Al_2O_3 from Aldrich, $Al(NO_3)_3$•$9H_2O$, reagent-grade aluminum nitrate from Acros, and pyrrole (C_4H_5N) from Acros (Germany). Potassium chloride KCl, cobalt chloride $CoCl_2$•$6H_2O$, and $FeCl_3$ $6H_2O$ in analytical grade and ethanol (CH_3CH_2OH) were procured from Sigma Aldrich were used for preparation of Cobalt aluminate $CoAl_2O_4$.

Synthesis techniques

Lithium aluminate $LiAlO_2$ in solid form and molten cobalt potassium chloride react to form cobalt aluminate $CoAl_2O_4$.

Synthesis of $LiAlO_2$

This initial material, which also contains $LiAlO_2$, was prepared via solid-state diffusion processes to create Lithium aluminate in commercial (reagent grade Aldrich). Dry ball milling for an hour produced powders of Li_2CO_3 and Al_2O_3 or Li_2CO_3 and $Al(NO_3)_3$ with a molar ratio of Li/Al=1. The nano-hydrated aluminum nitrate for the second mixture was first oven-dried at 1000C for 12 hours. Following that, the mixes are put into alumina crucibles and heated at a rate of 500oC. per hour in a muffle furnace with static air before being calcined for varied lengths of time at the selected reaction temperature. As a result, the γ-$LiAlO_2$, produced by calcining Li_2CO_3 + $2Al(NO_3)_3$ mixes at 900°C for 30 minutes, was chosen to produce $CoAl_2O_4$.

Preparation of the molten media for the chloride

$KCoCl_3$ was chosen as the double chloride in order to produce a chloride medium with Co_2+ ions that has a lower melting point than $CoCl_2$ (7240C). In the binary phase diagram, it is a definite chemical that melts incongruently at 362° C. In a pyrex container, KCl and $CoCl_2$•$6H_2O$ were immediately mixed in an equimolar ratio using a spatula. The mixture was oven for 12 hours at 150°C to dry it out. To make $KCoCl_3$, the compound was heated to 400 °C with air, melted under nitrogen flow for 15 minutes at a rate of 180 °C/h, then cooled to room temperature. The agate balls and container were milled with the solidified block for one hand before the powder was dried for one hour at 100°C in an oven. and maintained in a sealed glass container.

CoAl2O4 preparation

A 2.5 molar ratio of $KCoCl_3$ to $LiAlO_2$ was used to make cobalt aluminate., or Given that the chemical reaction occurs, the ratio should be five times the stoichiometric value. proceeds in accordance with Eq(1).

$$2LiAlO_2+KCoCl_3 \rightarrow CoAl_2O_4+2LiCl + KCl \qquad (1)$$

Before being put into the previously mentioned pyrex reaction tube of a vertical reactor, the chemicals were quickly mixed in a closed container by rotating movement. the rate of 1500 Ch-1, 450 or 5000C was used to heat the reaction mixture reaction temperature set and held for 12 hours. To prevent the excess $KCoCl_3$ from partially oxidizing into $Co3O_4$ during the thermal treatment, nitrogen flow (12 lh1) was used. The released gases bubbled in a sodium hydroxide solution. once cooled, the excess chlorides were removed from the $CoAl_2O_4$ water-insoluble oxide phase by water extraction, until no chloride ion was detected by AgCl precipitation, which took several water washing stages.

Synthesis of Ppy- $CoAl_2O_4$ polymer nanocomposite films

$FeCl_3.6H_2O$ is dissolved in distilled water to form a 0.5 M aqueous solution,10% $CoAl_2O_4$ (0.05 g) was disseminated and kefted for 30 minutes. The pyrrole monomer was then polymerized in the abovementioned mixture by adding 0.3 moles of pyrrole solution, which was then stirred for three hours to produce the composite. Other PPy samples were prepared with different weight percentages of $CoAl_2O_4$ (10, 20, 30, and 40%). The composites that are so produced are dried by being kept in an oven at 600C for a day. The paste was screen printed in the desired patterns onto a glass substrate. To remove the temporary binder, the films were burned at 2000C for two hours.

Characterization of Polypyrrole Thin Films Doped with CoAl2O4

Additional characterisation of the produced $CoAl_2O_4$ doped polypyrrole was carried out using films. X-ray-diffractometer (Ultima IV, Japan) CuKα radiation (λ =1.5405) was used to study the crystalline state of these films at a scanning rate of 0.02o per second at 40 mA and 40 kV. SEM microscopy was used to evaluate the morphological characteristics of the films (SEM, JSM-6360LV, Japan) operating at 120 kV. The chemical bonding was examined using FTIR spectroscopy and a Spectrum RXI make-model instrument from Perkin Elmer.A UV-VIS spectrophotometer operating between 200 and 1100 nm in wavelength was used to examine the films optical properties (Specord- 200 plus Germany). Using a programmable Keithley source metre, the current-voltage (I-V) characteristics of the films were examined (Keithley 2636A).

Gas sensing measurements

As a probe gas, ammonia is used, A digital multimeter is used to measure resistance, A digital thermometer with an alumel-chrome thermocouple is used to monitor the micro heater's temperature and a gas sensor unit is used to take measurements [16]. Our calculations show that the heater is originally connected to 12.5 V to set the oven's temperature, maintaining a constant temperature of 150 °C, and measuring the resistance of the sensor in the air. Over time, the sensor's resistance decreases, and this is recorded. The chamber is filled with an ammonia gas concentration that is known. The bottle is opened, and the sensor is positioned in the open air after choosing the value with the lowest constant resistance. It is now possible to track how resistance has changed over time. A comparable approach was used repeatedly (on films) on each sample under the exact same conditions [17,18].

Results and Discussion

X-ray diffraction study

As shown in figure 1a, the powder cobalt aluminate ($CoAl_2O_4$) X-ray's diffraction pattern was created from a mixture of KCoCl3 and $LiAlO_2$ with a molar ratio of 2.5. Figure 1b displays the PPy powder's XRD patterns. The PPy

powder sample's peak is mostly amorphous in nature. At roughly 2θ = 250, a broad peak was seen. The board peak, which is indicative of amorphous matter, points to PPy's short-range arrangement chains [19]. Figure 1c. shows the XRD peaks of all the CoAl2O4 polypyrrole films that were investigated. It can be seen that, in comparison to polypyrrole peaks, the peaks at 27-350 were widened by the addition of $CoAl_2O_4$ while the peak intensities were increased by the addition of $CoAl_2O_4$. Due to the emission of significant amounts of gases during annealing, Figure 1c demonstrates a shift in peak positions. The Scherrer formula D = Kλ /cosɵ is used to calculate the average grain size of the synthesized samples from the major diffraction peaks, where K is constant (K = 0.94), λ and is the wavelength (1.5406 A0).The crystallite size cause the Bragg angle ɵ to expand,β which is full width half maximum [20].The produced samples have an average grain size between 50 and 65 nm. The standard grain size reduces as the CoAl2O4 concentration rises when $CoAl_2O_4$ is partially substituted for polypyrrole [21].

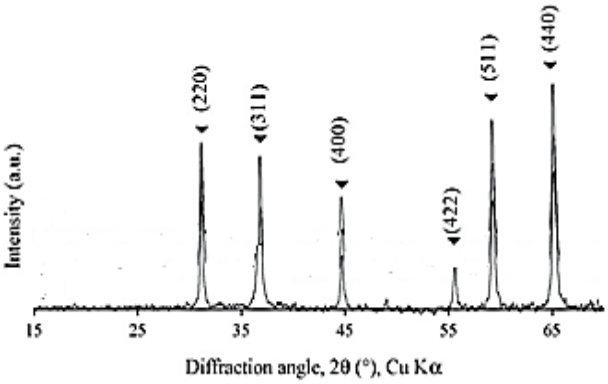

(a)

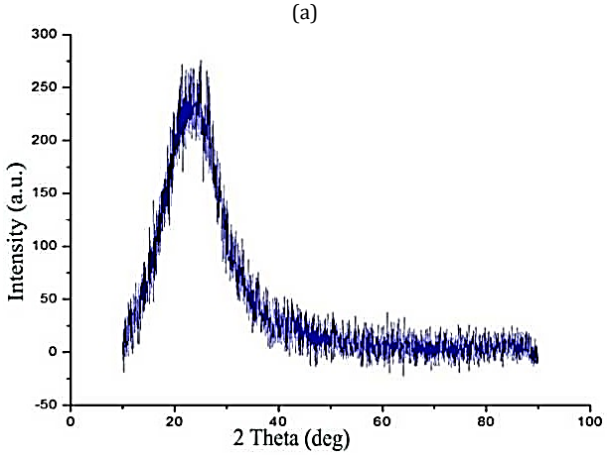

(b)

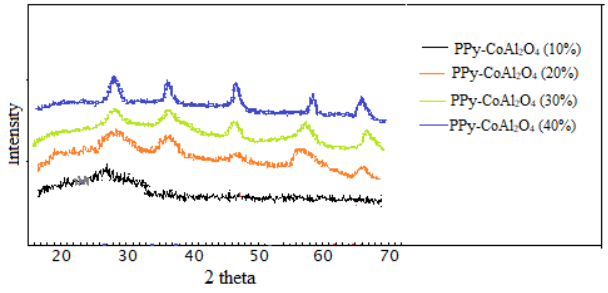

(c)

Figure 1: XRD pattern of (a) $CoAl_2O_4$, (b) PPy powder and (c) PPy-$CoAl_2O_4$ thin films

As shown in figure2c, the by weight percentage of pure PPy and Ppy-$CoAl_2O_4$ nanoparticle composites' FT-IR spectra (10, 20, 30 and 40 percent). The bulk PPy's spectra, as displayed in figure 2a, confirmed the synthesis of PPy.The IR spectrum of the powder $CoAl_2O_4$ was illustrated in the Fig.2(b), suggested the broad bands at 440, and 540-635 cm^{-1} were due to Li-Co and Al-O, vibrations respectively. The stretching vibration of C=C and C-C in the pyrrole ring is assumed to be caused by the band at 1550 cm^{-1} and the weak band at 1460 cm^{-1}[22-23].

At wavelengths of 1202 cm-1 and 1051 cm-1, respectively, the C-N and C-H stretching vibrations of pyrrole are readily discernible in the IR spectra of PPy [24]. The C-H in-plane deformation modes are related to the absorption at 1317 cm-1[25]. The bands at 920 cm-1 and 677 cm-1, respectively, may result from polymer N-H vibration and out-of-plane ring deformation [26, 27]. A considerable attenuation of the peak in the FT-IR spectrum of Ppy-CoAl2O4 nanoparticle composites loaded with by weight percent (10, 20, 30 and 40 percent) in Fig-2(c). suggests that PPy is a coating on every nanoparticle. The pyrrole ring's band at 1565cm-1 and 1475 cm-1 caused by the stretching modes of C=C and C-C has vanished, and a broad band has instead emerged at 1530 and 1490 cm-1 in concentrations of 10% and 20% of Ppy- CoAl2O4 nanoparticle, respectively. These notable alterations are related to a chemical reaction between PPy and CoAl2O4 nanoparticles, as percentage of dopant $CoAl_2O_4$ increases with PPy the bands appeared at 440 and 540-635 cm-1 were slightly shifted to higher frequencies due to involvement of $CoAl_2O_4$ nanoparticles in the formation of PPy- $CoAl_2O_4$ composite materials.

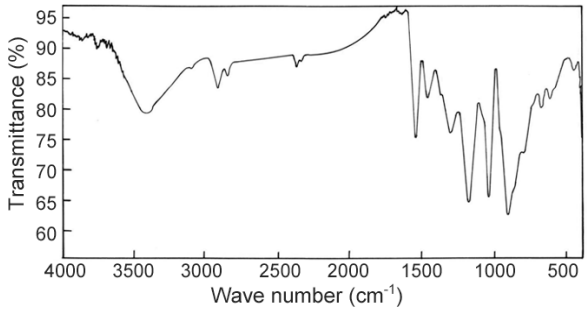

(a)

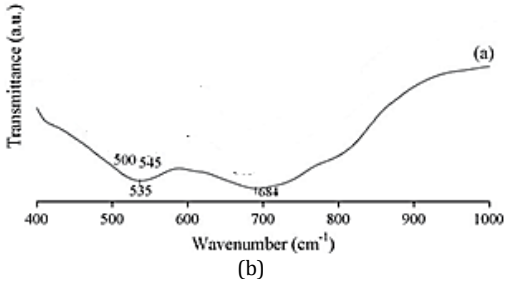

(b)

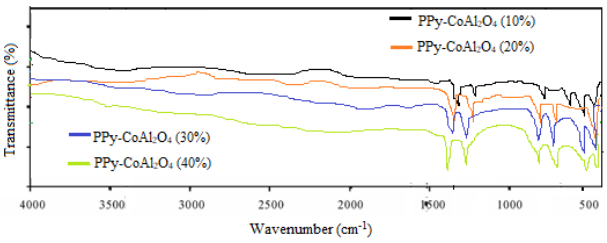

(c)

Figure 2: IR spectra of (a) polypyrrole films, (b) $CoAl_2O_4$ and (c) PPy- $CoAl_2O_4$ thin films

Morphology study using SEM

The SEM images for the composite films made of PPy-$CoAl_2O_4$ and $CoAl_2O_4$ are shown in Fig. 3. The SEM clearly distinguishes between the doped and undoped sample's microstructures. In general, the undoped Ppy has a greater granular structure than the doped one. The diameters of the granules were discovered to vary when dopants were utilised during the polymerization with polypyrrole. The PPy- $CoAl_2O_4$ films have a completely different morphology from the doped Ppy. For instance, as shown in Fig. 3, the microscopic $CoAl_2O_4$ particles that diffused into the layer of Ppy combine to form semi-spherical structures or grains. A thorough examination of the SEM may also reveal the appearance of tiny black holes or cavities in the microstructures of PPy- $CoAl_2O_4$ composites that are indicative of the emergence of comparable holes associated to the order-disorder transition in $CoAl_2O_4$, as seen by S. A. et al. [28]. These morphological characteristics are thought to be beneficial for gas sensing applications.

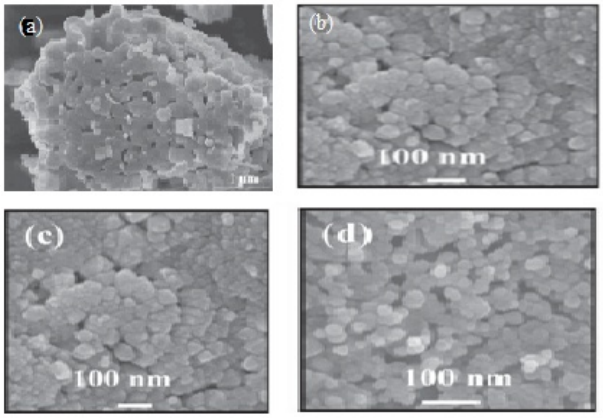

Figure 3: SEM images of (a) $CoAl_2O_4$, (b) PPy, (c) PPy-$CoAl_2O_4$ (20%), (d) PPy-$CoAl_2O_4$ (40%)

Optical properties

The optical properties of $CoAl_2O_4$ and PPy-$CoAl_2O_4$ samples were examined in the 300–1800 nm wavelength range, optical transmission (T) spectra are shown in Figure 4. (a). The increase in photon scattering brought on by the produced films' increased surface roughness is what is responsible for the lower transmittance of the films with higher SnMoO2 doping concentrations [29]. Figure 4 shows the optical absorption coefficient (α) of PPy- $CoAl_2O_4$ films with various $LiAlO_2$ doping contents (b). Beer-law Lambert's [30] provides an estimation of the absorption coefficient as follows:

$$\alpha = ln(1/T)(1/d)$$

where T is the transmittance and d is the film thickness. A film without PPy- $CoAl_2O_4$ has a thickness of 545 nm, and films doped with various amounts of Zn/TiO_2 have a thickness of 565 nm. It has been found that as the $CoAl_2O_4$ proportion rises, (α) increases while the wavelength (λ) drops. According to the association between incident photon energy (h) and absorption coefficient (α), the direct allowed energy band gap (Eg) of PPy- $CoAl_2O_4$ samples has been computed:

$$\alpha h\nu = A(h\nu - Eg)n$$

As shown in Fig. 4c, the optical band gap (Eg) value was computed by projecting the straight line segment of the curve to the (h) axis [31]. The results show that as $CoAl_2O_4$ doping levels rise, the optical band gap rises as well, which is consistent with differences in particle size. A well-known quantum confinement phenomenon known as the Burstein-Moss effect on band gap broadening causes the band gap to expand by reducing the particle size in addition to when the quantity of doping increases [32.33]. Additionally, structural disturbance in the lattice may alter the distribution of mid-level energy levels between the band's gaps, changing the Eg values. The rise in Eg suggests that PPy- $CoAl_2O_4$ films might be applied to optoelectronic components. The ratio known as the extinction coefficient (k) shows how quickly light intensity drops as it moves through a substance. In Fig. 4.d, the connection between k and wavelength is depicted, showing that k increased as the wavelength and $CoAl_2O_4$ content increased.

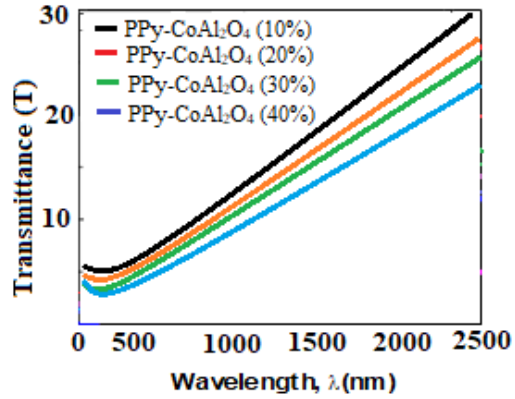

(a)

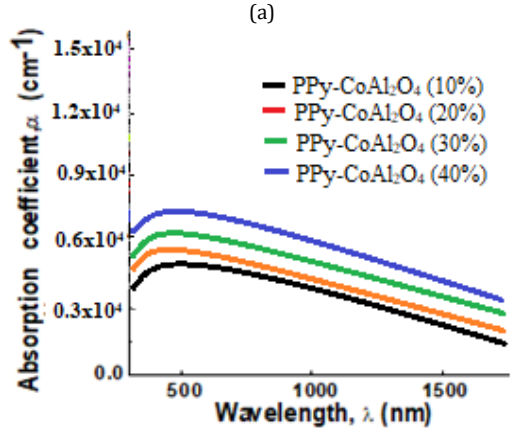

(b)

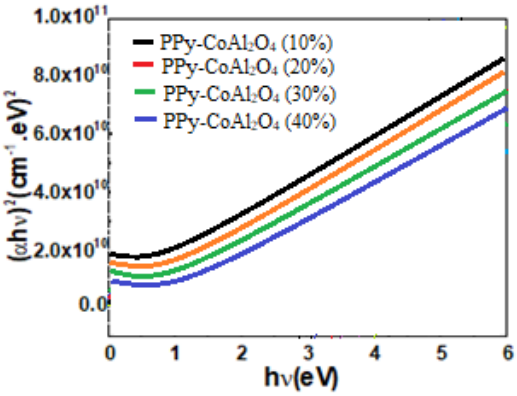

(c)

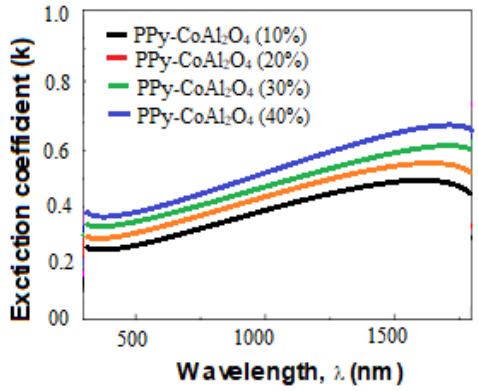

Figure 4: (a) Relation between transmission and wavelength, (b) Absorption coefficient Vs wavelength, (c) *(aht)2 Vs ht*, (d) Extinction coefficient against wavelength

Electrical conductivity measurement

As demonstrated in Table 1, the conductivity of PPy and the doped samples in pelletized powder is marginally lower than that of the PPy films cast from the solvents. This is as a result of the numerous kinds of structural problems that exist in PPy chains, which have a significant impact on the mobility of charge carriers and, ultimately, the conductivity of the polymer. Because $CoAl_2O_4$ changes the conducting network of PPy chains and introduces an ordered arrangement of the macromolecular chains, it will increase conductivity when added to the backbone of Ppy [34].

Table 1: Electrical conductivity of PPy and PPy- $CoAl_2O_4$ samples in pelletized form

Sample No	Sample Name	Conductivity in S/cm
1	PPy	2.34×10^{-3}
2	PPy- CoAl2O4 (10%)	3.25×10^{-2}
3	PPy- CoAl2O4 (20%)	4.55×10^{-2}
4	PPy- CoAl2O4 (15%)	5.62×10^{-2}
5	PPy- CoAl2O4 (20%)	6.84×10^{-2}
6	PPy- CoAl2O4 (25%)	7.56×10^{-2}

Gas Sensor

The ability to detect ammonia gas was tested on each sample of polypyrrole doped with $CoAl_2O_4$. A typical graph of current versus time for polypyrrole generated following exposure to ammonia gas is shown in Figure 5. Three tests were run on each sample to check the repeatability of the samples' absorption and desorption processes. Figure 5 shows the second and third cycles' current (I) vs. time charts to be somewhat different from the first cycle. This may be the situation because the desorption process took longer than expected to complete.

To calculate the sensitivity factor, use an equation.

$$S = \frac{Rg - Ro}{Ro}$$

where, Rg and Ro are, respectively, gas-filled and air-filled resistances. [35, 36] The results of the investigation's calculations for ammonia gas and $CoAl_2O_4$ doped polypyrrole sensors made utilizing various fabrication techniques.

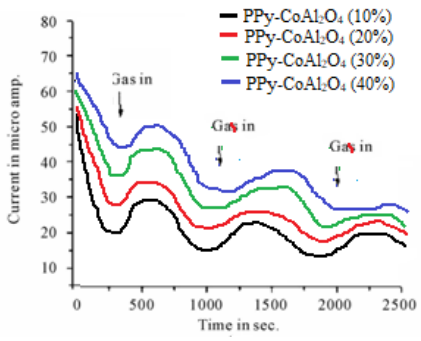

Figure 5: The response of different Ppy-$CoAl_2O_4$samples towards ammonia gas

It was demonstrated that different materials responded to ammonia gas in different ways for both pure Ppy and Ppy doped with ammonia. These tests revealed that a drop in current was observed when ammonia gas was exposed to $CoAl_2O_4$ doped Ppy that had been doped with varied weight percents of $CoAl_2O_4$ dopants. These $CoAl_2O_4$ doped Ppy have higher electrical conductivity than pure Ppy, which shows that the process produced a significant amount of charge carriers at high doping levels. Ammonia cannot generate more charges because the charge density is already higher; instead, it lowers the effective charge. Therefore, in this circumstance, Ppy's conductivity will drop, as has in fact been seen in our research. In conclusion, metal NPs can improve conducting polymers' capacity for sensing, mostly for the reasons indicated below first, the conductivity of polymers is changed by the addition of metal NPs. Second, certain kinds of metal NPs function as chemical receptors to increase sensor selectivity by having an affinity for specific gas molecules. By incorporating tiny metals into conductive polymers, the effective surface area of nanocomposites interacting with target gas is increased. Table 2 lists and summarises the prominent instances of sensors based on a hybrid system of conducting polymers and metal oxides that have been created in the last ten years. It was observed that as dopant ($CoAl_2O_4$) concentration increases the response of the PPy-$CoAl_2O_4$ composites were also increases.

Conclusions

Ppy-$CoAl_2O_4$ polymer nanocomposite thin films were prepared by chemical oxidation method. These notable alterations are related to a chemical reaction between PPy and $CoAl_2O_4$ nanoparticles observed in IR spectra of PPy-$CoAl_2O_4$, as percentage of dopant $LiAlO_2$ increases with PPy the bands appeared at 450, 540-655 and 810 cm^{-1} were slightly shifted to higher frequencies due to involvement of $CoAl_2O_4$ nanoparticles in the formation of PPy- $CoAl_2O_4$ composite materials. According to an XRD analysis, the diffraction peaks for $CoAl_2O_4$ doped polypyrrole grow more strong upon insertion into the polypyrrole matrix, indicating the well-crystalline character of the obtained Ppy-$CoAl_2O_4$ composite films. This XRD pattern also suggested that as dopant ($CoAl_2O_4$) percentage increases the sharpness of the peaks increases, hence composite materials change from amorphous to crystalline nature as dopant ($CoAl_2O_4$) concentration increases in polypyrrole matrix. The SEM demonstrates that the appearance of tiny black holes or cavities in the microstructures of the Ppy- $CoAl_2O_4$

Table 2: Conducting polypyrrole / metal oxides doped composites used in ammonia gas sensors

Metal oxide	Polymer	Concen (ppm)	Response	Response / recovery time (s)	T (^{0}C)	References
SnO_2	PPy	10.7	75	259	RT	[37]
ZnO	PPy	0.5	21	256	RT	[38]
Ag	PPy	10	0.54	--	RT	[39]
$AgSnO_2$	PPy	0.02	3.15	--	RT	[40]
$AuTiO_2$	PPy	0.02	3.2	--	RT	[40]
$CoAl_2O_4$(10%)	PPy	100	65	--	RT	Present Study
$CoAl_2O_4$ (20%)	PPy	100	77	--	RT	Present Study
$CoAl_2O_4$(30%)	PPy	100	79	--	RT	Present Study
$CoAl_2O_4$(40%)	PPy	100	81	--	RT	Present Study

composite is similar to the formation of such holes associated with the order-disorder transition in $CoAl_2O_4$. The optical properties of each sample were examined between the wavelengths of 300 and 1800 nm. The findings demonstrate that the optical band gap rises with increasing $CoAl_2O_4$ doping levels, which is commensurate with changes in particle size. The conductivity measurement shows that adding $CoAl_2O_4$ to the Ppy chain's backbone will increase conductivity because it modifies the chain's conducting network. For the purpose of detecting ammonia gas, all the $CoAl_2O_4$ doped polypyrrole samples were investigated. It was observed that as dopant ($CoAl_2O_4$) concentration increases the response of the PPy-$CoAl_2O_4$composites were also increases.

Acknowledgements:
The authors are thankful to Poojya Dr. Sharanbasvappa Appa, President sharanbasveshwar Vidya vardhak sangha, Kalaburagi, Registrar Dr. Anilkumar Bidve and Dean Dr. Laxmi Patil of Sharnbasva University, Kalaburagi, for encouragement during the process of carring out this work.

References

1. M. Dariel, L.H. Bennett, D.S. Lashmore, P. Lubitz, M. Rubinstein, W.L. Lechter, M.Z. Harford, Properties of electrodeposited Co-Cu multilayer structures, J. Appl. Phys., 61 (1987) 4067. https://doi.org/10.1063/1.338529
2. W.D. Williams, N. Giordano, Experimental study of localization and electron-electron interaction effects in thin Au wires, Phys. Rev. B, 33 (1986) 8146. https://doi.org/10.1103/PhysRevB.33.8146
3. T.M. Whitney, J.S. Jiang, P.C. Searson, C.L. Chien, Fabrication and magnetic properties of arrays of metallic nanowires, Science, 261 (1993) 1316. https://doi.org/10.1126/science.261.5126.1316
4. L. Piraux, J.M. George, J.F. Despres, C. Leroy, E. Ferain, R. Legras, K. Ounadjela, A. Fert, Giant magnetoresistance in magnetic multilayered nanowires, Appl. Phys. Lett., 65 (1994) 2484. https://doi.org/10.1063/1.112672
5. C. J. Brumlik, C. R. Martin, Anal. Chem., 59 (1992) 2625.
6. Z. Cai, C. R. Martin, Electronically conductive polymer fibers with mesoscopic diameters show enhanced electronic conductivities, J. Am. Chem. Soc., 111 (1989) 4138. https://doi.org/10.1021/ja00193a077
7. S.K. Chakarvarti, J. Vetter, Morphology of etched pores and microstructures fabricated from nuclear track filters, Nucl. Instruments Methods. B, 62 (1991) 109. https://doi.org/10.1016/0168583X(91)95936-8
8. S. K. Chakarvarti, J. Vetter, Microfabrication of metal-semiconductor heterostructures and tubules using nuclear track filters, J. Microm. Microeng., 3, (1993) 57.
9. S. K. Chakarvarti, J. Vetter, Template synthesis—a membrane based technology for generation of nano-/micro materials: a review, Radiat. Measur., 29(2) (1998) 149.
10. M. Hashim, Alimudin, S. Kumar, S.E. Shirsath, E. M. Mohamed, H. Chunge, et al., Studies on the activation energy from the ac conductivity measurements of rubber ferrite composites containing manganese zinc ferrite, Physica B, 407(21) (2012) 4097-103. https://doi.org/10.1016/j.physb.2012.06.006
11. Goldman A. Modern ferrite technology. 2nd ed. New York: Springer, (2006).
12. S. E. Shirsath , R. H Kadam., S. M. Patange, M. L. Mane, A. Ghasemi, A. Morisako, Enhanced magnetic properties of Dy3+ substituted Ni–Cu–Zn ferrite nanoparticles, Appl Phys Lett, 100 (2012) 042407-10. https://doi.org/10.1063/1.3679688
13. Narayanaswamy, N. Sivakumar, Influence of mechanical milling and thermal annealing on electrical and magnetic properties of nanostructured Ni–Zn and cobalt ferrites, Bull Mater Sci, 31, (2008) 373-80.
14. Hong L, Li Y, Yang M. Fabrication and ammonia gas sensing of palladium/polypyrrole nanocomposite. Sensor Actuat B-Chem. 2010;145:25–31.
15. Zhang J, Liu X, Wu S, et al. One-pot fabrication of uniform polypyrrole/Au nanocomposites and investigation for gas sensing. Sensor Actuat B-Chem. 2013;186:695–700.
16. M. Afzal, P.S.Naik, L.I.Nadaf, 2015, "Cost Effective Experimental Setup for Gas Sensing Applications", Journal of Applied Chamistry (8), PP, 37-44
17. Q. Wang, C. Wang, H. Sun, P. Sun, Y. Wang, J. Lin, G. Lu,2016," Microwave assisted synthesis of hierarchical Pd/SnO2nanostructures for CO gas sensor ", Sens. Actuator B—Chem. 222, PP, 257–263.
18. K.K. Khun, A. Mahajan, R. Bedi, 2011, "Surfactant assisted growth of nano structured tin oxide films for gas sensing applications", Electron. Mater. Lett. 7, PP, 303–308.
19. B. D. Cullity, "Elements of X-Ray Diffraction,"Addison-Wesley Publishing Company Inc., London, (1978).
20. Paoli M A D, Waltman R .J., Diaz A F., Bargon J., (1984). Conductive composites from poly (vinyl chloride) and polypyrrole J. Chem. Soc., Chem. Commu. 15, 1015–1016.

21. J Wang, S Chen, and M S Lin, (1989)., Use of different electropolymerization conditions for controlling the size-exclusion selectivity at polyaniline, polypyrrole and polyphenol films, Journal of Electro analytical Chemistry, 273,.1-2, 231–242. http://doi.org/10.1016/0022-0728(89)87016-0.
22. H. Kato, O. Nishikwa, T. Matsui, S. Honma and H. Kokado, "Fourier Transform Infrared Spectroscopy Study of Conducting Polymer Polypyrrole Higher Order Structure of Electrochemically Synthesized Film," The Journal of Physical Chemistry, 95,15, 6014- 6016, (1991). doi:10.1021/j100168a055
23. N. V. Bhat, A. P. Gadre and V. A. Bambole, "Structural, Mechanical and Electrical Properties of Electro polymerized Polypyrrole Composite Films," Journal of Applied Polymer Science, 80, 13, 2511-2517, (2001), doi:10.1002/app.1359
24. T. K. Vishnuvardhan, V. R. Kulkarni, C. Basavaraja and S. C. Raghavendra, "Synthesis, Characterization and A. C. Conductivity of Polypyrrole/Y2O3 Composites," Material Science, 29, 1, 77-83, (2006).
25. J Wang, S Chen, and M S Lin, Use of different electropolymerization conditions for controlling the size-exclusion selectivity at polyaniline, polypyrrole and polyphenol films, Journal of Electro analytical Chemistry, 273,.1-2, 231–242, (1989). http://doi.org/10.1016/0022-0728(89)87016-0.
26. El-Tantawy F, Abdelkader K M, Kane Ko F, Sung Y K. Physical properties of CdS-poly (vinyl alcohol) nanoconducting composite synthesized by organosol techniques and novel application potential, Eur. Polym. J. 40, 415, (2004). doi.org/10.1016/j.eurpolymj.2003.10.013
27. Mofokeng, S., Kumar, V., Kroon, R., Ntwaeaborwa, O., Structure and optical properties of Dy3+ activated sol-gel ZnO-TiO2 nanocomposites. J. Alloy. Compd. 711, 121–131, (2017)
28. El All, S.A., El-Shobaky, G.A., Structural and electrical properties of c-irradiated TiO2/Al2O3 composite prepared by sol–gel method. J. Alloy. Compd. 479 (1–2), 91–96, (2009)
29. C.M. Muiva, T.S. Sathiaraj, K. Maabong, Effect of doping concentration on the properties of aluminium doped zinc oxide thin films prepared by spray pyrolysis for transparent electrode applications. Ceram. Int. 37, 555–560 (2011). https://doi.org/10.1016/j.ceramint.2010.09.042
30. D.F. Swinehart, The beer-lambert law. J. Chem. Educ. 39(7), 333 (1962). https://doi.org/10.1021/ed039p333
31. S.A. Gad, H. Shaban, B.A. Mansour, G.M. Mahmoud, Determination and analysis of linear and nonlinear optical properties and electrical conductivity of amorphous PbxGe42-xSe48Te10 thin films. Appl. Phys. A 126, 354 (2020). https://doi.org/10.1007/s00339-020-3449-0
32. A.H. Omran Alkhayatt, S.K. Hussian, Fluorine highly doped nanocrystalline SnO2 thin films prepared by SPD technique. Mater. Lett. 155, 109–113 (2015). https://doi.org/10.1016/2F j.matlet.2015.04.130
33. J. Li, X. Liu, Preparation and characterization of a-MoO3 nanobelt and its application in supercapacitor. Mater. Lett. 112, 39–42 (2013). https://doi.org/10.1016/j.matlet.2013.08. 094
34. M. Trchova and J. Kova, Synthesis and structural study of polypyrroles prepared in the presence of surfactants, Synth. Met., 138(3) 447–455, (2003).
35. P P Sengupta, S Barik and B Adhikari, Polyaniline as a Gas-Sensor Material "Materials and Manufacturing Processes, 21,.3,.263–270,(2007). http://doi.org/10.1080/10426910500464602
36. Liu C, Hayashi K, Toko K. Au nanoparticles decorated polyaniline nanofiber sensor for detecting volatile sulfur compounds in expired breath. Sensor Actuat B-Chem. 2012;161:504–509.
37. Li Y, Ban H, Yang M. Highly sensitive NH3 gas sensors based on novel polypyrrole-coated SnO2 nanosheet nanocomposites. Sensor Actuat B-Chem. 2016;224:449–457.
38. Li Y, Jiao M, Yang M. In-situ grown nanostructured ZnO via a green approach and gas sensing properties of polypyrrole/ZnO nanohybrids. Sensor Actuat B-Chem. 2017;238:596–604.
39. Zhang J, Liu X, Wu S, et al. One-pot fabrication of uniform polypyrrole/Au nanocomposites and investigation for gas sensing. Sensor Actuat B-Chem. 2013;186:695–700.
40. Jiang T, Wang Z, Li Z, et al. Synergic effect within n-type inorganic–p-type organic nano-hybrids in gas sensors. J Mater Chem C. 2013;1:3017.
41. Tao qin, Guirong Li, Hongming Wang, Wenxue Su , Chao Dong, Jincheng Yu Microstructure and Properties of Microwave-Sintered Nd2Fe14Bp/2024 Aluminum-Alloy–Co Composites, October 2022 Crystals 12(10):1493. DOI:10.3390/cryst12101493